



This discussion paper is/has been under review for the journal Natural Hazards and Earth System Sciences (NHESS). Please refer to the corresponding final paper in NHESS if available.

Hydroelastic analysis of ice shelves under long wave excitation

T. K. Papathanasiou^{1,*}, A. E. Karperaki², E. E. Theotokoglou³, and K. A. Belibassakis²

¹Department of Civil Engineering and Surveying & Geoinformatics Engineering, Technological Educational Institute of Athens, Athens, Greece

²School of Naval Architecture and Marine Engineering, National Technical University of Athens, Zografou Campus, Athens, Greece

³Department of Mechanics, School of Applied Mathematical and Physical Science National Technical University of Athens, Zografou Campus, Athens, Greece

* now at: DICAM, University of Trento, via Mesiano 77, 38123 Trento, Italy

Received: 10 March 2015 – Accepted: 22 March 2015 – Published: 5 May 2015

Correspondence to: A. E. Karperaki (karperaki.ang@gmail.com)

Published by Copernicus Publications on behalf of the European Geosciences Union.

Hydroelastic analysis of ice shelves under long wave excitation

T. K. Papathanasiou et al.

Title Page

Abstract

Introduction

Conclusions

References

Tables

Figures



Back

Close

Full Screen / Esc

Printer-friendly Version

Interactive Discussion



Abstract

The transient hydroelastic response of an ice shelf under long wave excitation is analysed by means of the finite element method. The simple model, presented in this work, is used for the simulation of the generated kinematic and stress fields in an ice shelf, when the latter interacts with a tsunami wave. The ice shelf, being of large length compared to its thickness, is modelled as an elastic Euler–Bernoulli beam, constrained at the grounding line. The hydrodynamic field is represented by the linearised shallow water equations. The numerical solution is based on the development of a special hydroelastic finite element for the system of governing of equations. Motivated by the 2011 Sulzberger Ice Shelf (SIS) calving event and its correlation with the Honshu Tsunami, the SIS stable configuration is studied. The extreme values of the bending moment distribution in both space and time are examined. Finally, the location of these extrema is investigated for different values of ice shelf thickness and tsunami wave length.

1 Introduction

The catastrophic impact of climate change on the Antarctic Peninsula is examined in the works of Scambos et al. (2003) and Skvarca et al. (1999), where attempts to identify the mechanisms of climate-induced, ice shelf disintegration are made. Ice shelf stability is being re-evaluated as wave trains are becoming rougher and elevated temperatures lead to the further weakening of ice formations (Young et al., 2011). In fact, the question of whether ocean wave forcing acts as a collapse triggering mechanism is thoroughly explored in the literature. In particular, gravity wave forcing is depicted as a major cause of rift propagation within an ice shelf, preceding breakup events (Bromirski and Stephen, 2012). Additionally, the effects of infra-gravity waves and intense storm activity are also considered crucial for ice shelf stability (Bromirski et al., 2010).

NHESSD

3, 3057–3075, 2015

Hydroelastic analysis of ice shelves under long wave excitation

T. K. Papathanasiou et al.

Title Page

Abstract

Introduction

Conclusions

References

Tables

Figures

◀

▶

◀

▶

Back

Close

Full Screen / Esc

Printer-friendly Version

Interactive Discussion



attempts incorporate direct time integration schemes, Fourier transforms, modal expansion techniques and other methods (Meylan and Sturova, 2009; Sturova, 2009; Watanabe et al., 1998). Papathanasiou et al. (2015) developed a higher-order finite element for the time domain solution of the hydroelastic problem composed of a freely floating or semi-fixed body, over shallow bathymetry.

In the present contribution, the previous work of the authors on higher order FE schemes (i.e. Papathanasiou et al., 2015) will be applied in the hydroelastic analysis of ice-shelves under long-wave excitation. In Sect. 2 the physical domain and the governing equations are presented. The variational formulation of the previously defined initial-boundary value problem is discussed in Sect. 3. In Sect. 4 a case study, with parameters resembling that of the Sulzberger Ice shelf, is analyzed by means of the proposed methodology. The temporal distributions of the maximum and minimum bending moment values, along with their corresponding location along the semi-fixed floating body are given. Finally, a parametric analysis regarding the location of the occurred extreme bending moment values is performed for different ice shelf thickness and initial disturbance wavelength values.

2 Physical domain geometry and governing equations

The ice shelf is represented by an elastic, heterogeneous, thin plate with a fixed edge, extending infinitely at the y direction (vertical to the page). The plate of horizontal length L , rests on a layer of inviscid, incompressible fluid over an impermeable bottom. Assuming shallow water conditions, the long wave approximation (i.e. wavelength much greater than water depth) can be employed. The last assumption allows for dimensionality reduction, resulting in a 1-D system of equations, since now the z component of the fluid velocity is considered negligible. The domain is divided into regions $S_0 \equiv (0, L)$ and $S_1 \equiv (L, \infty)$, with the hydroelastic coupling taking place at the former (Papathanasiou et al., 2014). In S_0 , the plate deflection coincides with the water upper surface elevation $\eta(x, t)$. The fluid velocity potential in the two regions is denoted as φ_0 and φ_1 respec-

Hydroelastic analysis of ice shelves under long wave excitation

T. K. Papathanasiou et al.

Title Page

Abstract

Introduction

Conclusions

References

Tables

Figures



Back

Close

Full Screen / Esc

Printer-friendly Version

Interactive Discussion



The shear stress distribution, as derived from equilibrium relations, varies quadratically along the vertical direction. Maximum shear stress, located at the neutral fibre is,

$$\sigma_{xz}^{\max} = \frac{3}{2} \frac{V}{\tau/L} = \frac{3L}{2} \frac{K_x \eta_{xx} + K \eta_{xxx}}{\tau}, \quad (5)$$

The above system of equations is supplemented with boundary, interface and initial conditions. At the fixed end, simulating the ice shelf grounding line, the deflection and slope are set to zero. At the free edge of the plate, representing the ice shelf tip facing the ocean, zero bending moment and shear force is imposed. These conditions read

$$\eta(0, t) = \eta_x(0, t) = M_b(1, t) = V(1, t) = 0. \quad (6)$$

The water velocity is assumed zero underneath the grounding line and thus the velocity potential gradient vanishes,

$$\varphi_{0x}(0, t) = 0. \quad (7)$$

At the interface between S_0 and S_1 , assuming energy and mass conservation, the following matching conditions are derived (Stoker, 1957; Sturova, 2009)

$$B(1^-)\varphi_{0x}(1^-, t) = B(1^+)\varphi_{1x}(1^+, t) \text{ and } \dot{\varphi}_0(1^-, t) = \dot{\varphi}_1(1^+, t). \quad (8)$$

The ice shelf is assumed to be initially at rest, while an incoming long wave transverses region S_1 and reaches the free edge of the shelf. The initial boundary value problem formulation is thus completed with the following conditions,

$$\eta(x, 0) = \dot{\eta}(x, 0) = \varphi_{0x}(x, 0) = 0, \quad x \in S_0 \text{ and} \quad (9a)$$

$$\varphi_{1x}(x, 0) = 0, \dot{\varphi}_1(x, 0) = -F(x), \quad x \in S_1. \quad (9b)$$

In the last of Eq. (9b), $F(x)$ denotes the free surface elevation caused by the Tsunami wave at an initial time, at an area distant to the ice shelf edge.

Hydroelastic analysis of ice shelves under long wave excitation

T. K. Papathanasiou et al.

Title Page

Abstract

Introduction

Conclusions

References

Tables

Figures

◀

▶

◀

▶

Back

Close

Full Screen / Esc

Printer-friendly Version

Interactive Discussion



3 Finite elements – variational formulation of the governing equations

In order to derive the variational formulation of the above problem, Eqs. (1)–(3) are multiplied by the weight functions v , $-w_0$ and w_1 , respectively. Integration by parts yields,

$$5 \int_0^1 Mv\ddot{\eta}dx + \int_0^1 K v_{xx} \eta_{xx} dx + \int_0^1 v\eta dx + \int_0^1 v\dot{\varphi}_0 dx + [v(K\eta_{xx})_x]_0^1 + [v_x K \eta_{xx}]_0^1 = 0, \quad (10)$$

$$- \int_0^1 w_0 \dot{\eta} dx - [Bw_0 \varphi_{0x}]_0^1 + \int_0^1 Bw_{0x} \varphi_{0x} dx = 0, \quad (11)$$

$$10 \int_1^\infty w_1 \ddot{\varphi}_1 dx - [Bw_1 \varphi_{1x}]_1^\infty + \int_1^\infty Bw_{1x} \varphi_{1x} dx = 0. \quad (12)$$

Using the conditions described in Eqs. (6)–(8), and adding Eqs. (10)–(12) the equivalent semi-discrete variational problem is formulated as (Papathanasiou et al., 2015):

10 Find η , φ_0 and φ_1 , such that for every v , w_0 and w_1 at any given moment in time it holds

$$\int_0^1 M\ddot{\eta}^h v^h dx + \int_0^1 v^h \dot{\varphi}_0^h dx - \int_0^1 w_0^h \dot{\eta}^h dx + \int_1^\infty w_1^h \ddot{\varphi}_1^h dx + a(\eta^h, v^h) + b_0(w_0^h, \varphi_0^h) + b_1(w_1^h, \varphi_1^h) = 0, \quad (13)$$

where $a(\eta^h, v^h) = \int_0^1 (K v_{xx}^h \eta_{xx}^h + v^h \eta^h) dx$, $b_0(w_0^h, \varphi_0^h) = \int_0^1 Bw_{0x}^h \varphi_{0x}^h dx$, and

15 $b_1(w_0^h, \varphi_0^h) = \int_1^\infty Bw_{1x}^h \varphi_{1x}^h dx$, while superscript h denotes spatially discrete quantities.

stresses due to bending are dominant and as a first approach, shear stresses may be neglected. In Figs. 2 and 3 the maximum and minimum bending moment temporal and spatial distributions are shown. For the maximum bending moment, the temporal distribution is shown in a thick red line, while the location of the corresponding values along the ice shelf is given by the thin black line (Fig. 2). When at rest, the maximum bending moment is zero in absence of flexural effects. Immediately after impact, $t \approx 30$ the maximum bending moment is seen to increase. The location of the maximum bending moment value is found to follow the main pulse towards the fixed end. At $t = 34$, the entire pulse has passed underneath the floating cantilever, causing an increase in maximum bending moment. At the same time, the location of the maximum value for the bending moment is shifted back near the free edge. This is due to the fact that the entire wavelength of the initial pulse has passed underneath the floating cantilever, causing the tip to bend again as it recovers to the initial undeformed state. At $t = 44$ the location of the maximum bending moment value is shifted towards the ice shelf tip once again. The above can be attributed to flexural effects taking place at the right side of the propagating disturbance. As the hydroelastic wave propagates away from the free edge, the tip is restored to its original position causing additional flexing in the interior of the cantilever. Due to fact that, in the present work, the grounding line is simplistically modeled as a fixed boundary, the global bending moment extrema are found at the fixed edge, at the time of reflection $t = 67$. Prior to full reflection, a series of spikes in the maximum bending moment distribution are caused by the dispersed hydroelastic waves reaching the fixed edge before the main pulse.

As shown in Fig. 3, the minimum bending moment intensifies until the entire pulse wavelength has passed under the floating cantilever, at which point the minimum bending moment value remains virtually constant up to the arrival of the dispersed wavetrain at the fixed edge.

Notably, the notion that the pulse will reach the fixed end is rather unrealistic. The induced flexural effects will cause the bending failure of the semi-fixed floating body long before the hydroelastic pulse arrives at the grounding line. As seen in Figs. 2 and 3, the

NHESSD

3, 3057–3075, 2015

Hydroelastic analysis of ice shelves under long wave excitation

T. K. Papathanasiou et al.

Title Page

Abstract

Introduction

Conclusions

References

Tables

Figures



Back

Close

Full Screen / Esc

Printer-friendly Version

Interactive Discussion



maximum and minimum bending moment values reach a plateau approximately after the full disturbance passes underneath the ice shelf. Considering the effects before the hydroelastic wavetrain reaches the grounding line, namely for short times after the long wave impact, the corresponding location of the given extreme bending moment value along the ice shelf may be linked to both ice shelf thickness and initial disturbance form. Figure 4 displays a parametric study of the extreme bending moment value location for different ice shelf thickness and tsunami wavelength values. Variable ξ denotes the distance from the free edge up to the location of the extreme value along the semi-fixed floating body $x = 1$. In all cases, the extreme bending moment values have been considered in a time interval excluding the effects of the fixed end forcing ($t \geq 50$). In that manner, Fig. 4 demonstrates the location of extreme bending moments for the phase during which the main pulse enters the region of hydroelastic interaction. As can be seen in the aforementioned figure, the location of the extreme bending moment is relatively insensitive to variations of the wavelength. For thickness values of 80 and 100 m, this location is found to be at about 2% of the ice shelf length (2 km into the 100 km long ice shelf), calculated from the free edge. The above results are found in agreement with the work of Squire (1993), where the breakup of shore fast ice, modelled as a semi-infinite, thin floating plate, is investigated in the frequency domain. Furthermore, as thickness increases, the location of extreme values seems to shift towards the interior of the ice shelf. For a thickness of 120 m, location ξ is placed at approximately 10% of the ice shelf length and features a slight variation with increasing initial disturbance wavelength. However, this variation is very small when compared to the total length of the beam. Another interesting feature is that in this last case (120 m thickness) the maximum absolute value found corresponds to negative values of the bending moment (see Fig. 5), whereas for thickness values of 80 and 100 m the maximum absolute bending moment values are found to be positive (sagging moments). This feature explains the different shape of the 120 m curve in Fig. 4, when compared to the curves corresponding to 80 and 100 m, which closely resemble one another. The fact that in the case of 120 m the extreme bending moment values are negative might

Hydroelastic analysis of ice shelves under long wave excitation

T. K. Papathanasiou et al.

[Title Page](#)[Abstract](#)[Introduction](#)[Conclusions](#)[References](#)[Tables](#)[Figures](#)[Back](#)[Close](#)[Full Screen / Esc](#)[Printer-friendly Version](#)[Interactive Discussion](#)

be attributed to the beam thickness being very large compared to the water depth under the ice shelf. Finally, these results are strongly dependent on the form of the incoming wave, in the sense that if another wave profile instead of an elevation pulse is chosen, the bending moment fields will be of different nature.

5 Conclusions

In the present work, the transient hydroelastic response of a semi-fixed floating cantilever, resembling an ice shelf, is studied by means of a higher order finite element scheme. The simple model derived above is able to provide valuable information regarding the kinematic and stress fields induced by long wave forcing on an ice shelf. An illustrative case study is presented with parameters selected so as to approximately simulate the Sulzberger Ice Shelf topology and the relevant calving event conditions, initiated by the 2011 Honshu Tsunami. Bending moment profiles, as generated by a long wavelength elevation pulse, are studied and critical points of the induced stress field are located. During the wave entry in the hydroelasticity dominated region, the locations of extreme bending moments is found to be relatively insensitive to the excitation wavelength for given ice shelf thickness values. Important extensions of the present study include 3-D hydroelastic interaction, as well as the investigation nonlinearity effects of both in the hydrodynamic model and in the elastic subregion.

Acknowledgements. The present work has been supported by the project HYDELFS funded by the Operational Program “Education and Lifelong Learning” of the National Strategic Reference Framework (NSRF 2007-2013) -Research Funding Program ARHIMEDES-III: investing in knowledge society through the European Social Fund. In particular, author T. K. Papathanasiou acknowledges support from the aforementioned program for the period from 6 September 2012 to 30 September 2014.

Hydroelastic analysis of ice shelves under long wave excitation

T. K. Papathanasiou et al.

Title Page

Abstract

Introduction

Conclusions

References

Tables

Figures



Back

Close

Full Screen / Esc

Printer-friendly Version

Interactive Discussion



References

- Bhattacharjee, J. and Guedes Soares, C.: Flexural gravity wave over a floating ice sheet near a vertical wall, *J. Eng. Math.*, 75, 29–48, 2012.
- Brocklehurst, P., Korobkin, A. A., and Părău, E. I.: Interaction of hydro-elastic waves with a vertical wall, *J. Eng. Math.*, 68, 215–231, 2010.
- Bromirski, P. D. and Stephen, R. A.: Response of the Ross Ice shelf, Antarctica, to ocean-gravity wave forcing, *Ann. Glaciol.*, 53, 163–172, 2012.
- Bromirski, P. D., Sergienko, O. V., and MacAyeal, D. R.: Transoceanic infragravity waves impacting Antarctic ice shelves, *Geophys. Res. Lett.*, 37, L02502, doi:10.1029/2009GL041488, 2010.
- Brunt, K. M., Okal, E. A., and MacAyeal, D. R.: Antarctic ice shelf calving triggered by the Honsu (Japan) Earthquake and tsunami, March 2011, *J. Glaciol.*, 57, 785–788, 2011.
- Meylan, M. H. and Sturova, I. V.: Time-dependent motion of a two-dimensional floating elastic plate, *J. Fluid Struct.*, 25, 445–460, 2009.
- Papathanasiou, T. K., Karperaki, A., Theotokoglou, E. E., and Belibassakis, K. A.: A higher order FEM for time-domain hydroelastic analysis of large floating bodies in an inhomogeneous shallow water environment, *Proc. R. Soc. A*, 471, 20140643, doi:10.1098/rspa.2014.0643, 2015.
- Scambos, T., Hulbe, C., and Fahnestock, M.: Climate-Induced ice shelf disintegration in the Antarctic Peninsula, in: *Antarctic Peninsula Climate Variability: Historical and Paleoenvironmental Perspectives*, edited by: Domack, E., Levente, A., Burnet, A., Bind-schadler, R., Convey, P., and Kirby, M., American Geophysical Union, Washington, D.C., doi:10.1029/AR079p0079, 79–92, 2003.
- Sergienko, O. V.: Elastic response of floating glacier ice to impact of long-period ocean waves, *J. Geophys. Res.*, 115, F04028, doi:10.1029/2010JF001721, 2010.
- Skvarca, P., Rack, W., Rott, H., and Ibarzábal y Donángelo, T.: Climatic trend, retreat and disintegration of ice shelves on the Antarctic Peninsula: an overview, *Polar Res.*, 18, 151–157, 1999.
- Squire, V. A.: The breakup of shore-fast ice, *Cold Reg. Sci. Technol.*, 21, 211–218, 1993.
- Squire, V. A.: Of ocean waves and sea-ice revisited, *Cold Reg. Sci. Technol.*, 49, 110–133, 2007.

NHESSD

3, 3057–3075, 2015

Hydroelastic analysis of ice shelves under long wave excitation

T. K. Papathanasiou et al.

Title Page

Abstract

Introduction

Conclusions

References

Tables

Figures



Back

Close

Full Screen / Esc

Printer-friendly Version

Interactive Discussion



Hydroelastic analysis of ice shelves under long wave excitation

T. K. Papathanasiou et al.

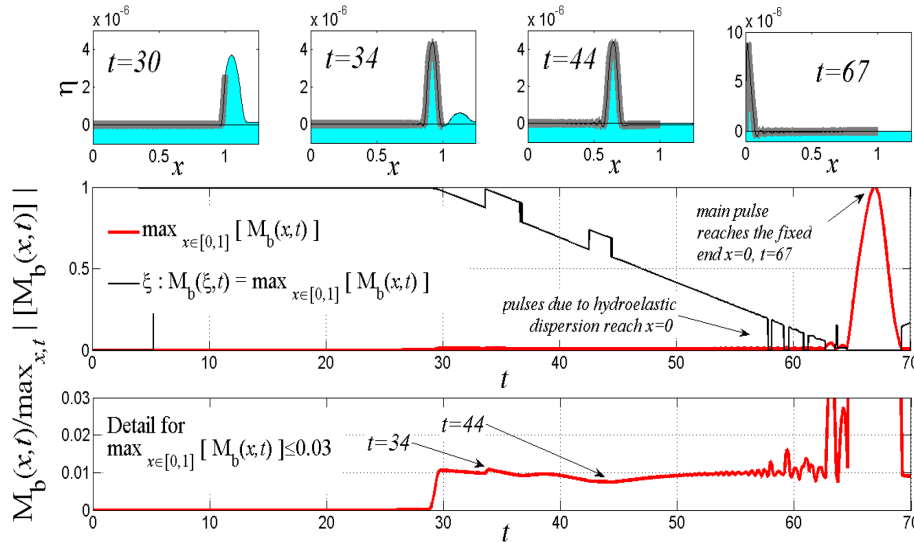


Figure 2. Maximum bending moment temporal profile (red thick line) and location of corresponding values along the floating cantilever (black line). A detailed figure of the profile after the wave impact is presented, along with representative snapshots of the deformed ice shelf.

Discussion Paper | Discussion Paper | Discussion Paper | Discussion Paper | Discussion Paper

Title Page

Abstract Introduction

Conclusions References

Tables Figures

◀ ▶

◀ ▶

Back Close

Full Screen / Esc

Printer-friendly Version

Interactive Discussion



Hydroelastic analysis of ice shelves under long wave excitation

T. K. Papathanasiou et al.

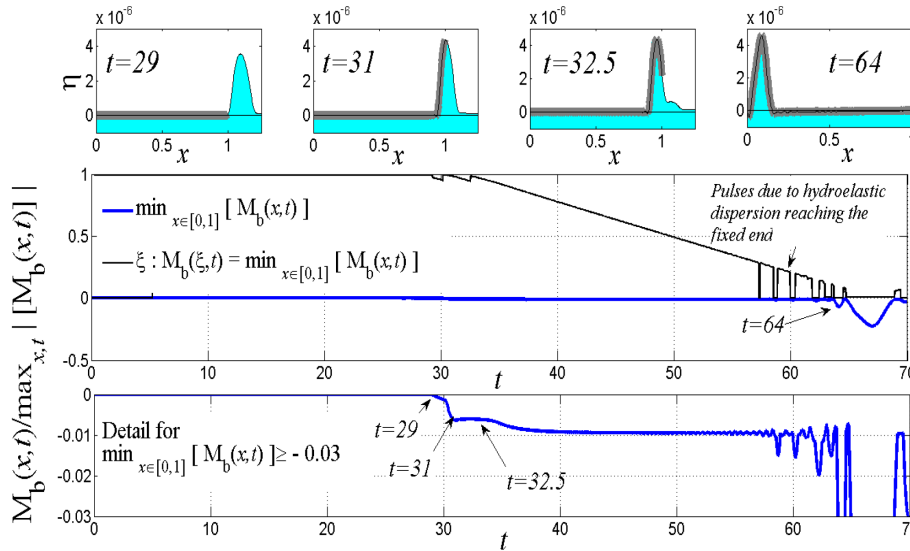


Figure 3. Minimum bending moment temporal profile (blue thick line) and location of corresponding values along the floating cantilever (black line). A detailed figure of the profile after the wave impact is presented, along with representative snapshots of the deformed ice shelf.

Discussion Paper | Discussion Paper | Discussion Paper | Discussion Paper | Discussion Paper

Title Page

Abstract

Introduction

Conclusions

References

Tables

Figures

◀

▶

◀

▶

Back

Close

Full Screen / Esc

Printer-friendly Version

Interactive Discussion



Hydroelastic analysis of ice shelves under long wave excitation

T. K. Papathanasiou et al.

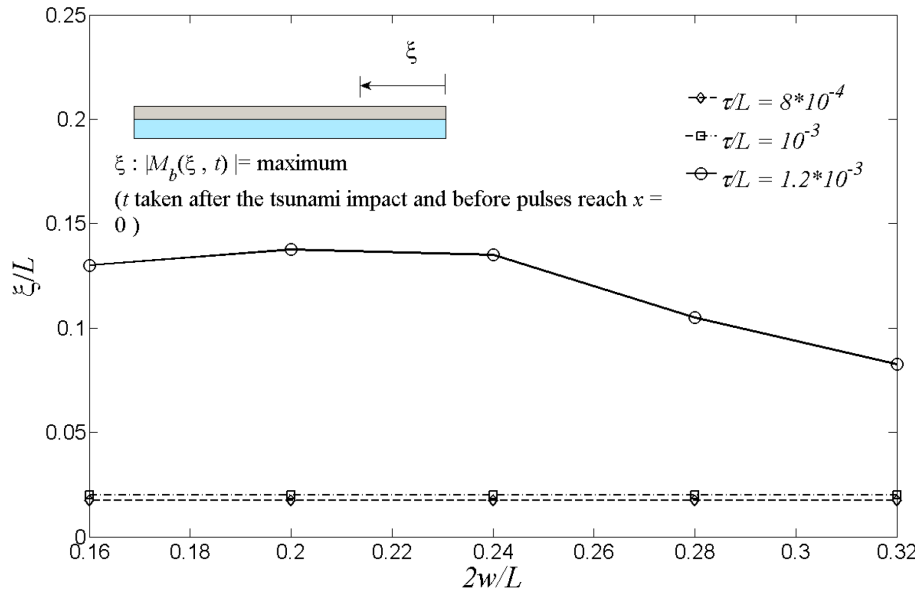


Figure 4. Location of extreme bending moment along the semi-fixed floating body for various values of thickness and initial disturbance wavelength. Variable ξ measures the distance of the point of occurrence of the extreme value from the free edge.

Title Page

Abstract Introduction

Conclusions References

Tables Figures

◀ ▶

◀ ▶

Back Close

Full Screen / Esc

Printer-friendly Version

Interactive Discussion



Hydroelastic analysis of ice shelves under long wave excitation

T. K. Papathanasiou et al.

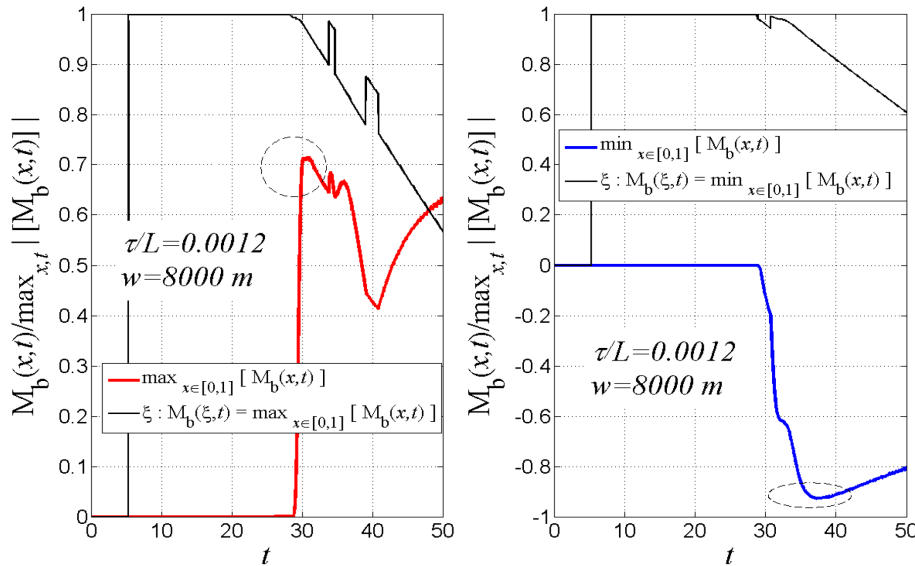


Figure 5. Plot of maximum and minimum bending moment value distributions for $w = 8000 \text{ m}$ and $\tau/L = 0.0012$. Extreme bending moment value is negative, during the entry phase, for an ice shelf thickness value of 120 m.

Title Page

Abstract

Introduction

Conclusions

References

Tables

Figures

◀

▶

◀

▶

Back

Close

Full Screen / Esc

Printer-friendly Version

Interactive Discussion

